"Edge/Basal Plane Half-Reaction Separation" Mechanism of Two-Dimensional Materials for Photocatalytic Water Splitting

*Yiran Ying, Zezhou Lin, and Haitao Huang**

Department of Applied Physics and Research Institute for Smart Energy, The Hong Kong Polytechnic University, Hung Hom, Kowloon, Hong Kong, P.R. China

AUTHOR INFORMATION

Corresponding Author

*E-mail: aphhuang@polyu.edu.hk

ABSTRACT. Two-dimensional (2D) materials are long considered as potential candidates for photocatalytic water splitting, but their applications are limited by high electron-hole recombination probability, low solar-to-hydrogen (STH) efficiencies, or 'catalyst poisoning' issues. Herein, we propose an 'edge/basal plane half-reaction separation' mechanism of 2D photocatalysts for water splitting for improving the photocatalytic efficiency. As a proof-of-concept, we design a group of stable and potentially exfoliable 2D rhodium chalcogenide halide (RhXY, X=S, Se, Te; Y=Cl, Br, I) photocatalysts with band gap values from 1.93 to 2.71 eV and suitable band edges. The half-reactions for photocatalytic water splitting, *i.e.*, hydrogen/oxygen evolution reaction (HER/OER), prefer to happen on the edge and basal planes of RhXY, respectively, and RhSCl, RhSeCl, and RhSeBr can also trigger HER and OER simultaneously without sacrificial reagents or cocatalysts. This work paves the way for the rational design of 2D photocatalysts with spatially separated half-reactions.

The past five decades have witnessed the unremitting development of photocatalytic water splitting techniques driven by solar energy ever since Fujishima and Honda discovered that TiO_2 can catalyze the reaction.[1] Nevertheless, most bulk oxide photocatalysts have too large band gap values (>3.0 eV) to effectively utilize visible light and near-infrared light, hindering the improvement of solar conversion efficiencies.[2, 3] In general, a promising highly efficient photocatalyst for overall water splitting should satisfy the following six criteria:[3, 4] (1) suitable band gap between 1.23 and 3.0 eV; (2) suitable band edge position to straddle the water redox potentials; (3) strong light harvesting ability; (4) efficient suppression of electron-hole recombination; (5) outstanding catalytic performance of the half-reactions of water splitting, *i.e.*,

hydrogen evolution reaction (HER) and oxygen evolution reaction (OER); and (6) high stability. Due to such restrictions, the exploration of highly efficient photocatalysts for water splitting is still a challenging topic.

Two-dimensional (2D) materials have recently emerged as promising photocatalysts for water splitting due to their merits including large surface area and short migration paths for charge carriers originating from their low-dimensional nature.[3-10] By means of theoretical calculations, a great many 2D materials, especially transition metal chalcogenides, have been predicted to possess suitable band structures for photocatalytic water splitting, including M_2X_3 (X=S, Se, Te),[11, 12] $MnPSe_3$,[13] GeX,[14-17] Janus transition metal dichalcogenides (TMDC),[18-21] $PdSeO_3$,[22] $Pd_3P_2S_8$,[23] Ge_4Se_9,[24] and $AgBiP_2Se_6$.[25] However, most reported 2D photocatalysts suffer from drawbacks including low solar-to-hydrogen (STH) efficiencies,[11, 26] the need for cocatalysts to trigger the HER/OER,[22] recombination of photogenerated electrons and holes,[4, 21] or difficult experimental synthesis, either of which could tremendously limit their practical applications. Furthermore, the competition between HER and OER active sites may induce the 'catalyst poisoning' issues and impedes the long-time performance of photocatalytic reactions, decreasing the efficiency of photocatalysts. The rational design of 2D photocatalysts which simultaneously solve all the challenges remains an urgent issue.

In previous works, the active sites investigated for 2D photocatalysts are limited to those on the basal planes, while the studies about those on the edge planes remain elusive. Actually, the edge sites of 2D TMDC (MoS_2) were proven to be the real active sites for electrocatalytic HER by experiments and theoretical calculations.[27, 28] Inspired by this, we try to design 2D photocatalysts whose HER and OER half-reactions proceed on the edge and basal planes separately, which can induce the spatial separation effect to improve photocatalytic efficiencies.

The 2D rhodium telluride chloride (RhTeCl) is recently predicted as a wide-band-gap semiconductor,[29-31] and can be potentially exfoliated from the RhTeCl crystals (reported in 1997).[32] The TMDC-like geometric structures with abundant chalcogenide sides and the wide-band-gap nature make rhodium chalcogenide halide monolayers potential candidates for photocatalysts with spatially separated HER and OER half-reactions.

In this work, we extend the 2D rhodium chalcogenide halides family to RhXY (X=S, Se, Te; Y=Cl, Br, I) and use state-of-the-art theoretical approaches to investigate their potential applications in photocatalytic water splitting. After a comprehensive screening by using stability, band gap, band edge positions, half-reaction performance, light absorption ability, and electron-hole separation ability as filters (**Scheme 1**), we identify three of them (RhSCl, RhSeCl, and RhSeBr) to be promising water splitting photocatalysts without the need for sacrificial reagents or cocatalysts. Most importantly, we propose an 'edge/basal plane half-reaction separation' mechanism based on the spatially separated active sites for HER and OER on the edge and basal planes, respectively, increasing the efficiency of the half-reactions and endowing 2D RhXY with great promise for future photocatalytic applications.

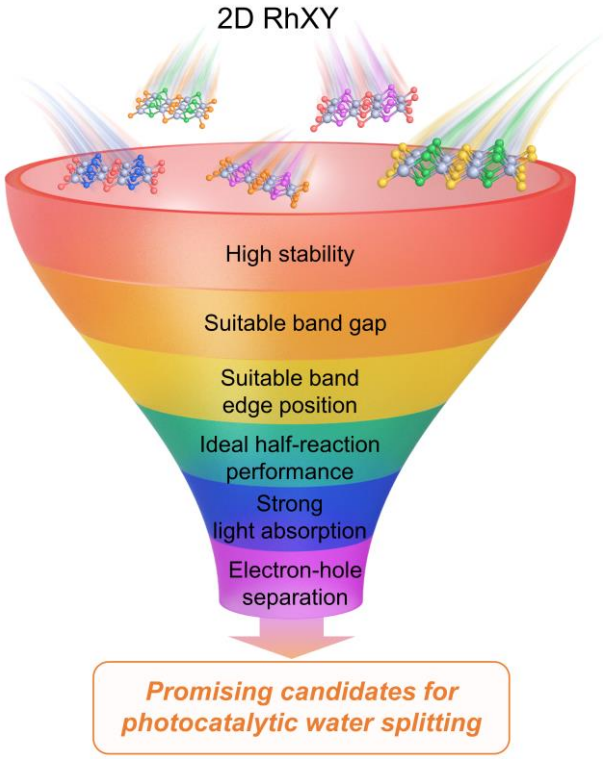

Scheme 1. The screening process of 2D RhXY as photocatalysts for water splitting based on the general requirements.

A representative geometric structure of 2D RhXY with the space group of P21/m (No. 11) is shown in **Figure 1**a, which exhibits similar geometric structures to 1T-phase TMDC with ABC stacking, but half of the chalcogen atoms in the A and C layers are replaced by halide atoms, forming distorted RhX_3Y_3 octahedrons. The electron localization function (ELF) in Figure S1 exhibits that Rh atoms form covalent bonds with X (S/Se/Te) atoms (ELF close to 0.5) while the bonds between Rh and Y (Cl/Br/I) are partially ionic (ELF<0.5), and electrons are localized around both X and Y atoms. All the RhXY monolayers exhibit cohesive energies (E_{coh}) values larger than 4.0 eV/atom (Table S1), suggesting that their formation is potentially feasible in experiments.[11]

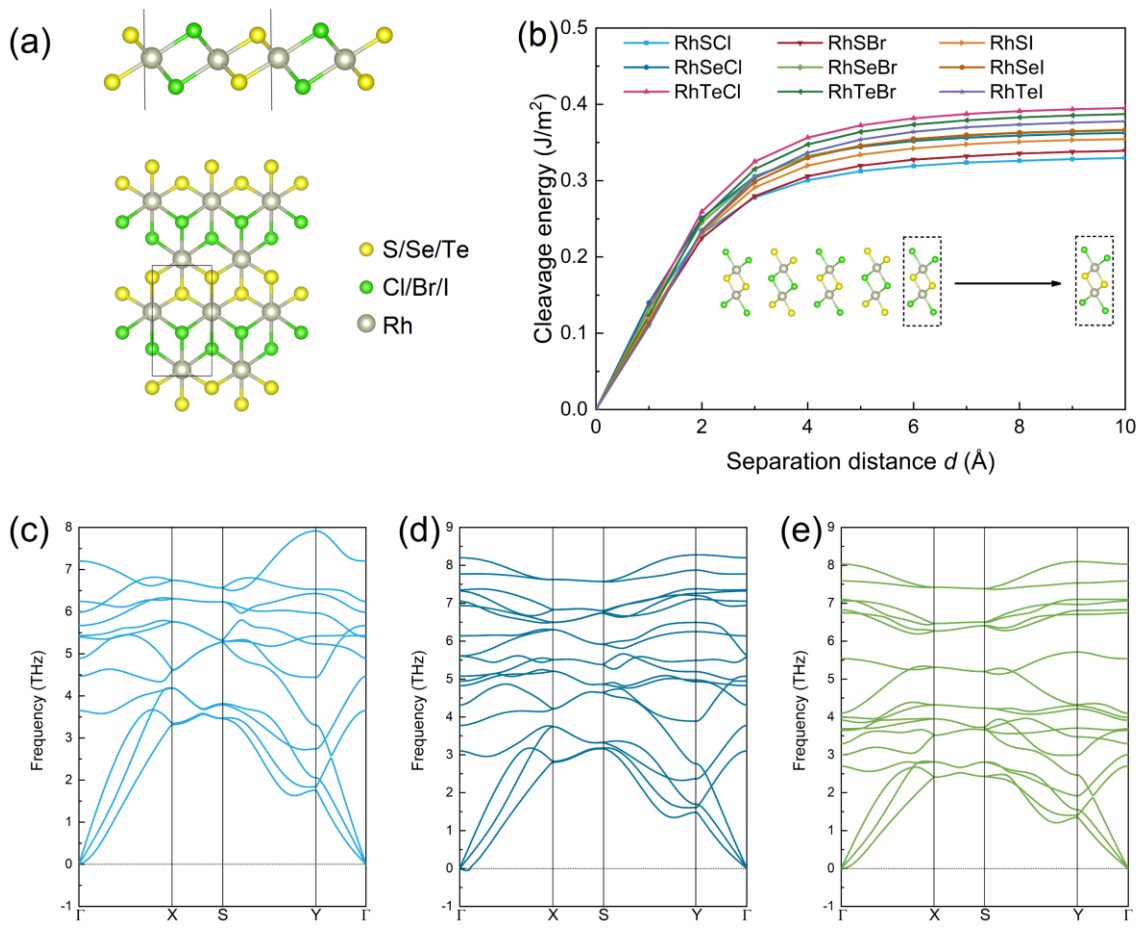

Figure 1. (a) Side and top views of the representative geometric structure of 2D RhXY, (b) cleavage energy as a function of separation distance *d* for 2D RhXY (inset shows an example of the cleavage process of the RhXY monolayer from quintuple layers), and phonon dispersion spectra calculated by density functional perturbation theory for 2D (c) RhSCl, (d) RhSeCl, and (e) RhSeBr.

Mechanical or chemical exfoliation is a common approach to obtain 2D materials from their bulk counterparts,[33, 34] and such possibilities are explored by calculating the cleavage energies. Results in Figure 1b show that cleavage energies converge to values between 0.33 J/m^2

(RhSCl) and 0.40 J/m^2 (RhTeCl); such values are close to or smaller than most of the common exfoliable 2D materials (Note S1 in the Supporting Information), indicating that 2D RhXY can be also synthesized by exfoliation. It should be noted that only bulk RhTeCl was synthesized experimentally by chemical transport reaction with elemental Rh, Te powder in Cl_2 flux,[32] and the synthesis of other RhXY is promising by using similar approaches, as confirmed by the reaction energy calculations (Table S1). Before investigating the photocatalytic activities for 2D RhXY, stability is a prerequisite. First, the phonon dispersion spectra are calculated to investigate the dynamic stability of 2D RhXY. Results in Figure 1c-e and Figure S2 show no imaginary frequencies in the whole Brillouin zone, and near the Γ point, the optical and acoustic branches are well-separated, indicating that RhXY monolayers are dynamically stable. *Ab initio* molecular dynamics (AIMD) simulations indicate that they are thermally stable (Figure S3) and can resist environmental O_2 attacking (Figure S4). The in-plane elastic constants (Table S2) satisfy the Born-Huang criteria[35] for all nine 2D RhXY structures, indicating their mechanical stability. We also observe the mechanical anisotropy in RhXY (Figure S5).

To avoid possible underestimation of the band gap,[36] HSE06 hybrid functional is used to obtain the electronic band structures of 2D RhXY. The band edge positions relative to the vacuum level are calculated and plotted in **Figure 2**a. The nine RhXY monolayers possess band gap values ranging from 1.93 eV (RhTeI) to 2.71 eV (RhSeCl), their conduction band minimum (CBM) positions are all higher than -4.44 eV (potential for H^+/H_2), and their valence band maximum (VBM) positions are all lower than -5.67 eV (potential for O_2/H_2O) (Figure 2a, Table S3). These results indicate that all nine RhXY systems satisfy the band requirements for efficient photocatalysts for water splitting. The moderate-band-gap feature can ensure high light harvesting efficiency and adequate driving force for water splitting, and the suitable band edge

positions can ensure that they can straddle the water redox potentials to provide a solar-driven driving force for the water splitting half-reactions, i.e., HER and OER. For practical applications, the 2D RhXY may exist as bilayers (Figure S6a). Our HSE06 calculations further prove that although RhXY bilayers have smaller band gap values (1.41-2.46 eV) than their monolayer counterparts, eight of them except for RhTeI can still satisfy the requirements (Figure S6b).

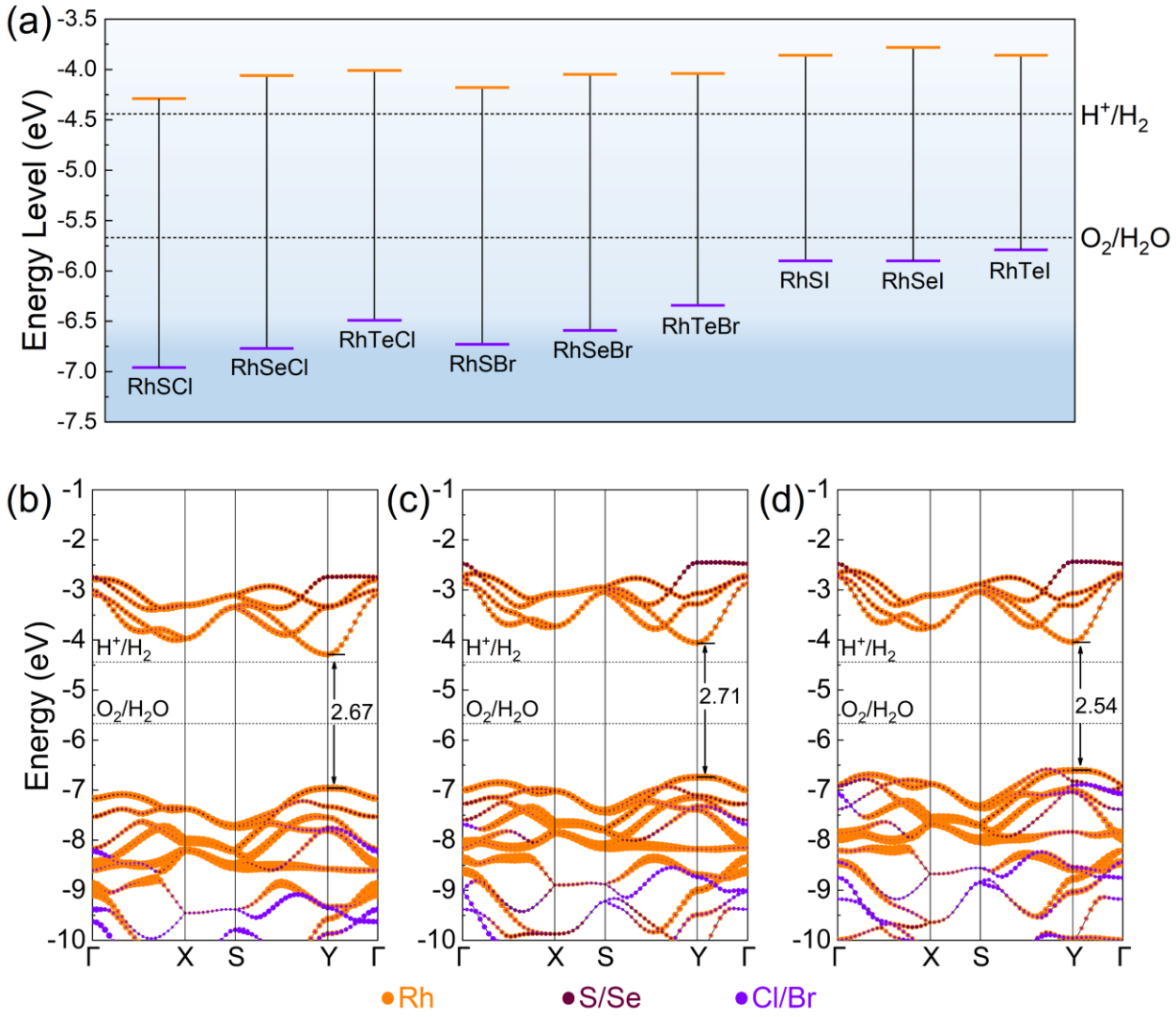

Figure 2. (a) The band edge positions of 2D RhXY relative to the vacuum level compared with the water redox potentials (pH=0), and the characteristic band structures calculated with HSE06

hybrid functional for (b) RhSCl, (c) RhSeCl, and (d) RhSeBr. The sizes of the dots in the figures are proportional to the weight of the projections of different atoms. Band gap values in eV are marked in (b)-(d).

We further investigate their band structures, as shown in Figure 2b-d and S7, five monolayers (RhSCl, RhSeCl, RhTeCl, RhSBr, and RhSeBr) are direct band gap semiconductors with CBM and VBM both at Y point; the other four possess indirect band gap feature, but the differences between indirect and direct band gap are smaller than 300 meV (Table S3), benefiting the photogenerated carriers.[37] The characteristic band structures (Figure 2b-d and S7) and the projected density of states (DOS, Figure S8) imply that the major contributions to the bands near the VBM and CBM are from Rh 4*d* orbitals, while the contributions from X and Y atoms are smaller. Nevertheless, for the iodide monolayers, iodine atoms have larger contributions to the VBM, making it deviates from the Y point to points on the Y→S path. Such a phenomenon eventually leads to the change of semiconductor type from direct to indirect for these monolayers. The spatial distribution of VBM and CBM is further visualized through the band-decomposed charge density distribution for 2D RhXY (Figure S9). The VBM of RhXY originates from the top regions of X atoms and top/bottom regions of Rh atoms, while the CBM is contributed by side regions of Rh, X atoms and bottom regions of Y atoms. Moreover, the variation of VBM and CBM positions for different RhXY monolayers can be attributed to the different strengths of the Rh-X bonds, where the VBM/CBM positions move higher when the Rh-X bond strength decreases (Figure S10), and since VBM has a larger linear response to bond strength than CBM, the band gap values of RhXY increase with stronger Rh-X bonds. In addition, compressive biaxial strain can make the band edge positions shift upwards for 2D

RhXY (Figure S11), and under 5% compressive strain, RhSCl, RhSeCl, RhSBr, RhSeBr, and RhTeBr can readily provide adequate driving forces for both HER and OER at pH=7 (Figure S11b).

The potentials from the photogenerated carriers can be directly utilized as the driving force for HER and OER half-reactions for water splitting. The potentials provided by photogenerated electrons U_e and photogenerated holes U_h are calculated as the difference between hydrogen reduction potential and CBM/VBM, respectively (Table S4).[22] We first investigate the HER thermodynamics on 2D RhXY. HER on the basal plane of 2D RhXY is not favorable (Figure S12-13). In contrast, the (100) edge plane of RhXY (Figure S14a) is highly HER-active with small ΔG_{*H} values from -0.35 to 0.30 eV (**Figure 3**a-c and S15), and under the light-on condition ($U=U_e$), both steps in HER become downhill in Gibbs free energy for RhXY, implying that HER becomes spontaneous. This hydrogen stabilization effect can be attributed to the low-coordination nature of the edge sites, which can enhance the interactions between H and the catalyst surface through the dangling bonds. H prefers to be adsorbed on S sites for RhSCl and RhSI, while H on Rh sites is more stable for the other systems; CBM is contributed by both active sites (Figure S14b-d), so the photogenerated electrons can trigger HER directly. Specifically, 2D RhSCl and RhSeCl exhibit ΔG_{*H} values of -0.02 and 0.09 eV at U=0, respectively, very close to the ideal value of zero as well as Pt(111) benchmark (-0.04 eV),[38, 39] indicating that their edge planes possess outstanding HER activities. In comparison, the two monolayers have inferior HER performance on (010) edge planes due to strong hydrogen adsorption on S/Se sites (Figure S16).

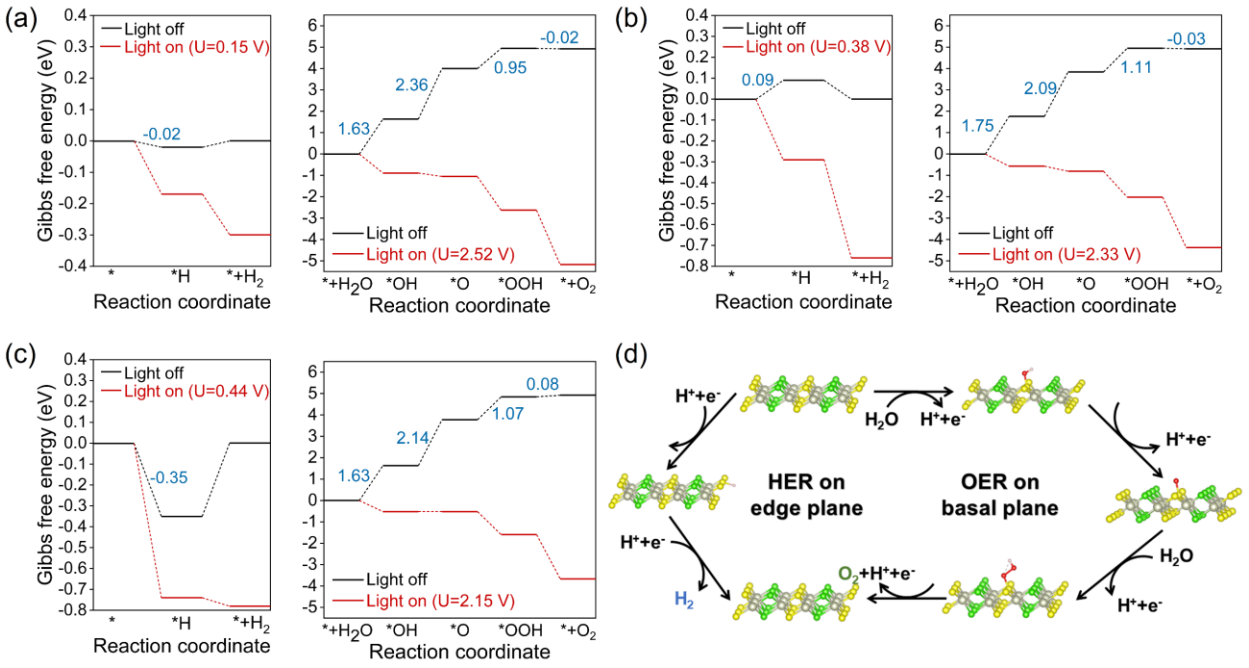

Figure 3. HER Gibbs free energy diagrams (left panel) under zero potential and applied potentials corresponding to U_e and OER Gibbs free energy diagrams (right panel) under zero potential and applied potentials corresponding to U_h for (a) RhSCl, (b) RhSeCl, and (c) RhSeBr monolayers. The solvation effect is included in the calculations by the implicit solvation model. (d) Schematic illustration of the spatially separated half-reactions on 2D RhXY. Color code for atoms: Rh in grey; X in yellow; Y in green; O in red; H in pale pink.

Next, the OER performance on the basal planes of 2D RhXY is studied. During the four-electron process under the light-off situation (U=0), the second step (*OH→*O+H^++e^-) is the potential-limiting step (PLS) for eight RhXY monolayers except for RhSeI (Figure 3a-c and S17), and the ΔG values range from 1.68 eV (RhSeI) to 2.36 eV (RhSCl). Interestingly, three of them (RhSCl, RhSeCl, and RhSeBr) possess larger U_h values than ΔG values of the PLS, and under the light-on situation (U=U_h), all the elementary steps in OER can be exothermic (Figure 3a-c). Combined with their HER activities, both HER and OER can proceed on these

photocatalysts spontaneously without the need for any sacrificial reagents or cocatalysts.[22] For other monolayers, the U_h is not enough to trigger the OER spontaneously, so cocatalysts are needed. The OER active sites on the basal planes are X-sites, coinciding with the regions where VBM locate (Figure S8). In addition, the OER process on the (100) edge plane of RhSCl, RhSeCl, and RhSeBr is much suppressed with high η_{OER} values (Figure S18), which suggests that OER on the edge plane cannot be initiated by the photogenerated potentials. We summarize the case of water splitting half-reactions on RhXY in a spatially separated manner (Figure 3d): HER happens on the edge plane while OER proceeds on the basal plane. This feature guarantees that there will be no competition between the active sites of HER and OER, benefiting the increase of water splitting efficiencies. RhSCl and RhSeCl bilayers can also catalyze the half-reactions through this mechanism (Figure S6c-d). Such an "edge/basal plane separation mechanism" can be extended to other 2D catalysts with different edge/basal plane catalytic selectivity for bifunctional applications.

For practical photocatalytic applications, the stability of 2D RhXY in aqueous solution under illumination is also evaluated. The calculated thermodynamic reduction potentials (φ_r) are all higher than that for H^+/H_2, and the oxidation potentials (φ_o) are all lower than that for O_2/H_2O (Note S2, Table S5-S6), indicating that RhXY can resist photoinduced corrosion.[40] The thermal stability in acidic solutions is also confirmed by AIMD simulations (Figure S19).

Strong light absorption ability is another requirement for efficient photocatalysts. To include the excitonic effect, GW with Bethe-Salpeter equation (BSE) calculations are performed on 2D RhXY to calculate the frequency-dependent dielectric function and therefore obtain the optical absorption spectra.[41-43] Results in **Figure 4a** indicate that: (1) all the 2D RhXY systems exhibit pronounced light absorbance coefficient values in the whole visible light region (380-750

nm), comparable to other reported photocatalysts (Note S3). (2) The optical absorption spectra of 2D RhXY are highly anisotropic, which originate from their geometric anisotropy. The absorbance along the *x*-direction is much stronger than the *y*-direction in the visible light region, and the trend is reversed in the ultraviolet region, together contributing to the strong light harvesting ability in both regions.

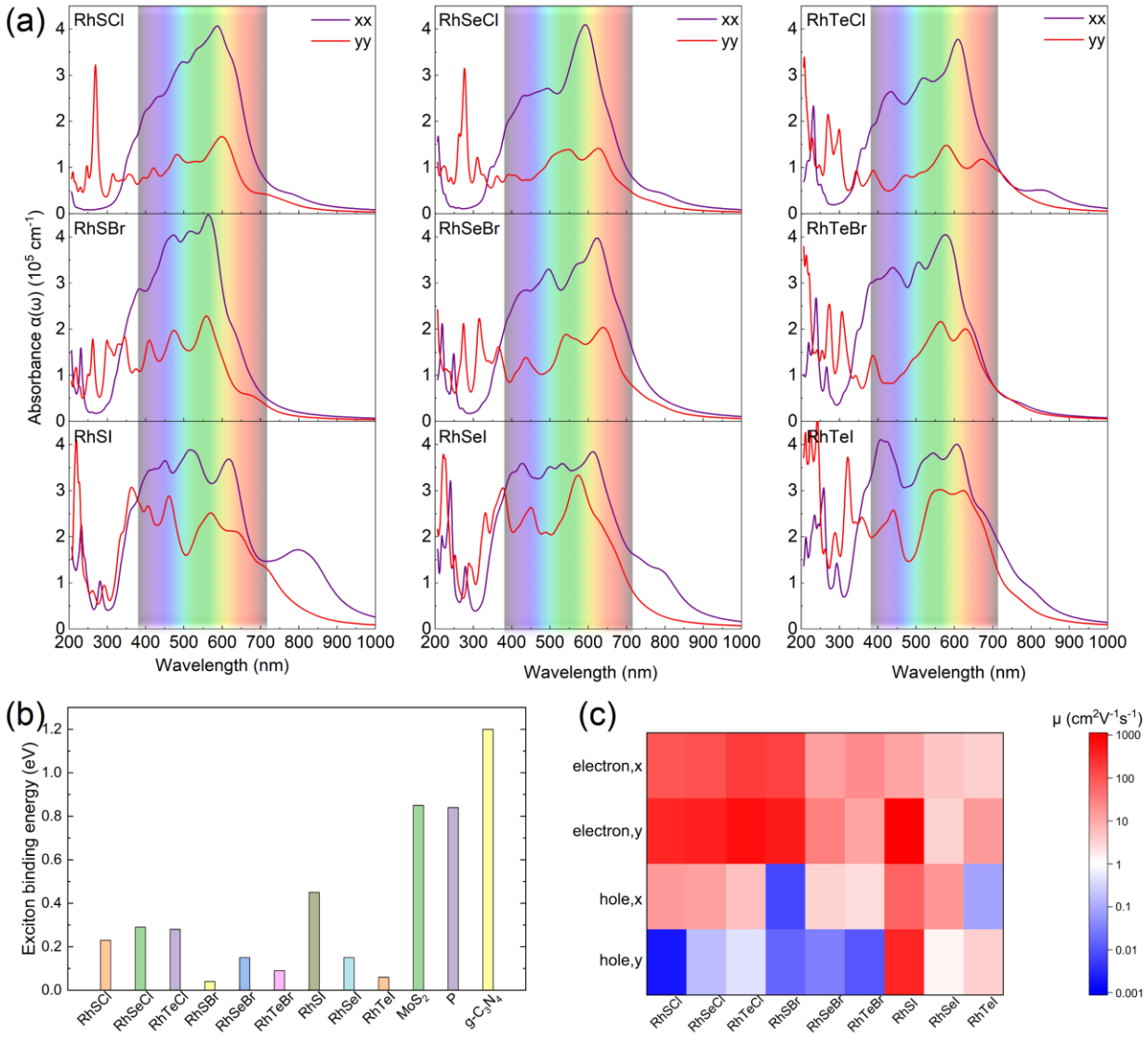

Figure 4. (a) Optical absorption spectra α(ω) and (b) exciton binding energies E_b (with comparisons to literature-reported values for 2D MoS_2, phosphorene, and g-C_3N_4)[44-46] of 2D

RhXY calculated by GW+BSE method. (c) Heatmap for electron and hole mobilities along *x*- and *y*-directions (in-plane) for 2D RhXY calculated by deformation potential theory.

The effective separation of electron-hole pairs is also a crucial factor for photocatalyst design. The exciton binding energy E_b is defined as the difference between GW-calculated quasi-particle band gap and the GW+BSE-calculated optical band gap[47, 48] and can be used to estimate the possibility of electron-hole recombination. Except for RhSI, the other eight RhXY monolayers possess ultrasmall E_b ranging from 0.04 eV (RhSBr) to 0.29 eV (RhSeCl) (Figure 4b), which are smaller than other reported 2D semiconductors (Table S7), indicating that photogenerated electrons and holes in 2D RhXY can be easily separated, benefiting photocatalysis. As for carrier mobilities, the electron mobilities are 1-2 orders of magnitude higher than the hole mobilities for most monolayers (Figure 4c, Table S8). Considering the smaller number of edge sites for HER than the number of basal sites for OER in large 2D flakes, higher electron mobilities can compensate for this and improve the kinetics of HER induced by the photogenerated electrons. All these features can contribute to the separation of electron-hole pairs on 2D RhXY and facilitate the transport of electrons to the HER active sites.

Finally, we calculate the STH efficiency η_{STH} of 2D RhXY as $\eta_{STH} = \eta_{abs} \times \eta_{cu}$,[11] where η_{abs} and η_{cu} are the efficiencies for light absorption and carrier utilization, respectively (detailed methods can be found in the Supporting Information). Results in Table 1 show that 2D RhXY exhibits high STH efficiencies ranging from 15.0% to 23.6%, higher than previously reported 2D photocatalysts such as $AgBiP_2Se_6$ (10.0%),[25] Janus WSSe (11.7%),[20] heptazine-based framework (12.0%)[26] and comparable to 2D M_2X_3 (2.6-32.1%),[11] indicating that RhXY monolayers are

highly efficient photocatalysts. Similar results (15.0% to 24.3%) are obtained if cocatalysts are used (Table S9).

Table 1. $\chi(H_2)$, $\chi(O_2)$, the energy of photons utilized for water splitting E, efficiency for light absorption η_{abs}, efficiency for carrier utilization η_{cu}, and STH efficiencies η_{STH} for 2D RhXY.

	$\chi(H_2)$/eV	$\chi(O_2)$/eV	E/eV	η_{abs}/%	η_{cu}/%	η_{STH}/%
RhSCl	0.15	1.29	2.67	42.8	37.8	16.2
RhSeCl	0.38	1.10	2.71	40.9	37.4	15.3
RhTeCl	0.44	0.82	2.72	51.0	29.4	15.0
RhSBr	0.26	1.06	2.56	48.5	38.1	18.5
RhSeBr	0.39	0.92	2.54	48.9	38.7	18.9
RhTeBr	0.40	0.67	2.58	59.5	30.4	18.1
RhSI	0.58	0.23	2.38	70.5	31.9	22.5
RhSeI	0.67	0.23	2.34	67.1	34.9	23.4
RhTeI	0.58	0.12	2.33	74.8	31.6	23.6

In summary, we theoretically predicted a group of 2D RhXY (X=S, Se, Te; Y=Cl, Br, I) to be promising photocatalysts for water splitting. The RhXY monolayers are wide-band-gap semiconductors (1.93-2.71 eV) with suitable band edge positions, strong light absorption in the whole visible-light region, theoretical stabilities, and can be potentially exfoliated from the corresponding bulk structures. More importantly, the HER and OER half-reactions of water splitting prefer to occur on the edge plane and basal plane of RhXY separately, greatly increasing the reaction efficiencies. Among all the systems, RhSCl, RhSeCl, and RhSeBr can trigger both

HER and OER spontaneously under the potentials provided by the photogenerated carriers, suggesting no need for cocatalysts. In addition, RhXY monolayers exhibit high electron-hole separation abilities (small exciton binding energies) and STH efficiencies (>15%). This work paves the way for the development of 2D photocatalysts for water splitting with spatially separated half-reactions and can be extended to the design of other highly efficient 2D catalysts with bifunctional catalytic activities.

ASSOCIATED CONTENT

Supporting Information. Computational methods, structural parameters, electron localization function, phonon dispersion spectra, energy and temperature fluctuation during AIMD simulations, elastic constants, band gap and band edge information, band structures, the density of states, band-decomposed charge density distribution, adsorption sites at the basal and edge planes, HER and OER Gibbs free energy diagrams at different sites, exciton binding energies, carrier mobilities, relaxation time, and STH efficiencies with cocatalysts for RhXY monolayers. (PDF)

AUTHOR INFORMATION

Corresponding Author

*aphhuang@polyu.edu.hk

Author Contributions

The manuscript was written through contributions of all authors. All authors have given approval to the final version of the manuscript.

Notes

The authors declare no conflict of interest.

ACKNOWLEDGMENT

This work was supported by the Research Grants Council of the Hong Kong Special Administrative Region, China (Project No. PolyU152140/19E) and the Hong Kong Polytechnic University (Q-CDBG and 1-W19S).

REFERENCES

1. Fujishima, A.; Honda, K., Electrochemical photolysis of water at a semiconductor electrode. *Nature* **1972,** *238* (5358), 37.

2. Chen, X.; Shen, S.; Guo, L.; Mao, S. S., Semiconductor-based photocatalytic hydrogen generation. *Chem. Rev.* **2010,** *110* (11), 6503-6570.

3. Fu, C.-F.; Wu, X.; Yang, J., Theoretical design of two-dimensional visible light-driven photocatalysts for overall water splitting. *Chem. Phys. Rev.* **2022,** *3* (1), 011310.

4. Singh, A. K.; Mathew, K.; Zhuang, H. L.; Hennig, R. G., Computational Screening of 2D Materials for Photocatalysis. *J. Phys. Chem. Lett.* **2015,** *6* (6), 1087-1098.

5. Tan, C.; Cao, X.; Wu, X. J.; He, Q.; Yang, J.; Zhang, X.; Chen, J.; Zhao, W.; Han, S.; Nam, G. H.; Sindoro, M.; Zhang, H., Recent Advances in Ultrathin Two-Dimensional Nanomaterials. *Chem. Rev.* **2017,** *117* (9), 6225-6331.

6. Zhao, Y.; Zhang, S.; Shi, R.; Waterhouse, G. I. N.; Tang, J.; Zhang, T., Two-dimensional photocatalyst design: A critical review of recent experimental and computational advances. *Mater. Today* **2020,** *34*, 78-91.

7. Wan, Y.; Wang, L.; Xu, H.; Wu, X.; Yang, J., A Simple Molecular Design Strategy for Two-Dimensional Covalent Organic Framework Capable of Visible-Light-Driven Water Splitting. *J. Am. Chem. Soc.* **2020,** *142* (9), 4508-4516.

8. Jing, Y.; Zhou, Z.; Geng, W.; Zhu, X.; Heine, T., 2D Honeycomb-Kagome Polymer Tandem as Effective Metal-Free Photocatalysts for Water Splitting. *Adv. Mater.* **2021,** *33* (21), 2008645.

9. Zhou, Z.; Springer, M. A.; Geng, W.; Zhu, X.; Li, T.; Li, M.; Jing, Y.; Heine, T., Rational Design of Two-Dimensional Binary Polymers from Heterotriangulenes for Photocatalytic Water Splitting. *J. Phys. Chem. Lett.* **2021,** *12* (33), 8134-8140.

10. Ganguly, P.; Harb, M.; Cao, Z.; Cavallo, L.; Breen, A.; Dervin, S.; Dionysiou, D. D.; Pillai, S. C., 2D Nanomaterials for Photocatalytic Hydrogen Production. *ACS Energy Lett.* **2019,** *4* (7), 1687-1709.

11. Fu, C. F.; Sun, J.; Luo, Q.; Li, X.; Hu, W.; Yang, J., Intrinsic Electric Fields in Two-dimensional Materials Boost the Solar-to-Hydrogen Efficiency for Photocatalytic Water Splitting. *Nano Lett.* **2018,** *18* (10), 6312-6317.

12. Zhao, P.; Ma, Y.; Lv, X.; Li, M.; Huang, B.; Dai, Y., Two-dimensional III_2-VI_3 materials: Promising photocatalysts for overall water splitting under infrared light spectrum. *Nano Energy* **2018,** *51*, 533-538.

13. Zhang, X.; Zhao, X.; Wu, D.; Jing, Y.; Zhou, Z., $MnPSe_3$ Monolayer: A Promising 2D Visible-Light Photohydrolytic Catalyst with High Carrier Mobility. *Adv. Sci. (Weinh)* **2016,** *3* (10), 1600062.

14. Lv, X.; Wei, W.; Sun, Q.; Li, F.; Huang, B.; Dai, Y., Two-dimensional germanium monochalcogenides for photocatalytic water splitting with high carrier mobility. *Appl. Catal., B* **2017,** *217*, 275-284.

15. Ji, Y.; Yang, M.; Dong, H.; Hou, T.; Wang, L.; Li, Y., Two-dimensional germanium monochalcogenide photocatalyst for water splitting under ultraviolet, visible to near-infrared light. *Nanoscale* **2017,** *9* (25), 8608-8615.

16. Qiao, M.; Chen, Y.; Wang, Y.; Li, Y., The germanium telluride monolayer: a two dimensional semiconductor with high carrier mobility for photocatalytic water splitting. *J. Mater. Chem. A* **2018,** *6* (9), 4119-4125.

17. Gu, D.; Tao, X.; Chen, H.; Zhu, W.; Ouyang, Y.; Peng, Q., Enhanced photocatalytic activity for water splitting of blue-phase GeS and GeSe monolayers via biaxial straining. *Nanoscale* **2019,** *11* (5), 2335-2342.

18. Ma, X.; Wu, X.; Wang, H.; Wang, Y., A Janus MoSSe monolayer: a potential wide solar-spectrum water-splitting photocatalyst with a low carrier recombination rate. *J. Mater. Chem. A* **2018,** *6* (5), 2295-2301.

19. Guan, Z.; Ni, S.; Hu, S., Tunable Electronic and Optical Properties of Monolayer and Multilayer Janus MoSSe as a Photocatalyst for Solar Water Splitting: A First-Principles Study. *J. Phys. Chem. C* **2018,** *122* (11), 6209-6216.

20. Ju, L.; Bie, M.; Tang, X.; Shang, J.; Kou, L., Janus WSSe Monolayer: An Excellent Photocatalyst for Overall Water Splitting. *ACS Appl. Mater. Interfaces* **2020,** *12* (26), 29335-29343.

21. Gao, X.; Shen, Y.; Liu, J.; Lv, L.; Zhou, M.; Zhou, Z.; Feng, Y. P.; Shen, L., Boosting the photon absorption, exciton dissociation, and photocatalytic hydrogen- and oxygen-evolution reactions by built-in electric fields in Janus platinum dichalcogenides. *J. Mater. Chem. C* **2021,** *9* (42), 15026-15033.

22. Qiao, M.; Liu, J.; Wang, Y.; Li, Y.; Chen, Z., $PdSeO_3$ Monolayer: Promising Inorganic 2D Photocatalyst for Direct Overall Water Splitting Without Using Sacrificial Reagents and Cocatalysts. *J. Am. Chem. Soc.* **2018,** *140* (38), 12256-12262.

23. Jing, Y.; Heine, T., Two-dimensional $Pd_3P_2S_8$ semiconductors as photocatalysts for the solar-driven oxygen evolution reaction: a theoretical investigation. *J. Mater. Chem. A* **2018,** *6* (46), 23495-23501.

24. Zhou, Y.; Zhou, L.; He, J.; Frauenheim, T., Inartificial Two-Dimensional Ge_4Se_9 Janus Structures with Appropriate Direct Band Gaps and Intrinsic Polarization Boosted Charge Separation for Photocatalytic Water Splitting. *J. Phys. Chem. Lett.* **2020,** *11* (8), 3095-3102.

25. Ju, L.; Shang, J.; Tang, X.; Kou, L., Tunable Photocatalytic Water Splitting by the Ferroelectric Switch in a 2D $AgBiP_2Se_6$ Monolayer. *J. Am. Chem. Soc.* **2020,** *142* (3), 1492-1500.

26. Zhao, Y.; Wang, C.; Han, X.; Lang, Z.; Zhao, C.; Yin, L.; Sun, H.; Yan, L.; Ren, H.; Tan, H., Two-Dimensional Covalent Heptazine-Based Framework Enables Highly Photocatalytic Performance for Overall Water Splitting. *Adv. Sci. (Weinh)* **2022,** *9* (28), 2202417.

27. Hinnemann, B.; Moses, P. G.; Bonde, J.; Jørgensen, K. P.; Nielsen, J. H.; Horch, S.; Chorkendorff, I.; Nørskov, J. K., Biomimetic hydrogen evolution: MoS_2 nanoparticles as catalyst for hydrogen evolution. *J. Am. Chem. Soc.* **2005,** *127* (15), 5308-5309.

28. Jaramillo, T. F.; Jørgensen, K. P.; Bonde, J.; Nielsen, J. H.; Horch, S.; Chorkendorff, I., Identification of active edge sites for electrochemical H_2 evolution from MoS_2 nanocatalysts. *Science* **2007,** *317* (5834), 100-102.

29. Mounet, N.; Gibertini, M.; Schwaller, P.; Campi, D.; Merkys, A.; Marrazzo, A.; Sohier, T.; Castelli, I. E.; Cepellotti, A.; Pizzi, G.; Marzari, N., Two-dimensional materials from high-throughput computational exfoliation of experimentally known compounds. *Nat. Nanotechnol.* **2018,** *13* (3), 246-252.

30. Zhou, J.; Shen, L.; Costa, M. D.; Persson, K. A.; Ong, S. P.; Huck, P.; Lu, Y.; Ma, X.; Chen, Y.; Tang, H., 2DMatPedia, an open computational database of two-dimensional materials from top-down and bottom-up approaches. *Sci. Data* **2019,** *6* (1), 86.

31. Ying, Y.; Fan, K.; Zhu, S.; Luo, X.; Huang, H., Theoretical Investigation of Monolayer RhTeCl Semiconductors as Photocatalysts for Water Splitting. *J. Phys. Chem. C* **2020,** *124* (1), 639-646.

32. Köhler, J.; Urland, W., RhTeCl–das erste Chalkogenidhalogenid eines Platinmetalls mit Schichtstruktur. *Z. Anorg. Allg. Chem.* **1997,** *623* (1-6), 583-586.

33. Novoselov, K. S.; Jiang, D.; Schedin, F.; Booth, T.; Khotkevich, V.; Morozov, S.; Geim, A. K., Two-dimensional atomic crystals. *Proc. Natl. Acad. Sci. U. S. A.* **2005,** *102* (30), 10451-10453.

34. Butler, S. Z.; Hollen, S. M.; Cao, L.; Cui, Y.; Gupta, J. A.; Gutiérrez, H. R.; Heinz, T. F.; Hong, S. S.; Huang, J.; Ismach, A. F., Progress, challenges, and opportunities in two-dimensional materials beyond graphene. *ACS Nano* **2013,** *7* (4), 2898-2926.

35. Mouhat, F.; Coudert, F.-X., Necessary and sufficient elastic stability conditions in various crystal systems. *Phys. Rev. B* **2014,** *90* (22), 224104.

36. Heyd, J.; Peralta, J. E.; Scuseria, G. E.; Martin, R. L., Energy band gaps and lattice parameters evaluated with the Heyd-Scuseria-Ernzerhof screened hybrid functional. *J. Chem. Phys.* **2005,** *123* (17), 174101.

37. Liu, L.; Jiang, B.; Sun, D.; Liu, H.; Xie, Y., Ab initio high-throughput screening of transition metal double chalcogenide monolayers as highly efficient bifunctional catalysts for photochemical and photoelectrochemical water splitting. *J. Mater. Chem. A* **2022,** *10* (26), 14060-14069.

38. Ma, L.; Li, Q.; Ying, Y.; Ma, F.; Chen, S.; Li, Y.; Huang, H.; Zhi, C., Toward Practical High-Areal-Capacity Aqueous Zinc-Metal Batteries: Quantifying Hydrogen Evolution and a Solid-Ion Conductor for Stable Zinc Anodes. *Adv. Mater.* **2021,** *33* (12), 2007406.

39. Seh, Z. W.; Kibsgaard, J.; Dickens, C. F.; Chorkendorff, I.; Norskov, J. K.; Jaramillo, T. F., Combining theory and experiment in electrocatalysis: Insights into materials design. *Science* **2017,** *355* (6321), eaad4998.

40. Chen, S.; Wang, L.-W., Thermodynamic Oxidation and Reduction Potentials of Photocatalytic Semiconductors in Aqueous Solution. *Chem. Mater.* **2012,** *24* (18), 3659-3666.

41. Salpeter, E. E.; Bethe, H. A., A Relativistic Equation for Bound-State Problems. *Phys. Rev.* **1951,** *84* (6), 1232-1242.

42. Bickers, N. E.; Scalapino, D. J.; White, S. R., Conserving approximations for strongly correlated electron systems: Bethe-Salpeter equation and dynamics for the two-dimensional Hubbard model. *Phys. Rev. Lett.* **1989,** *62* (8), 961-964.

43. Albrecht, S.; Reining, L.; Del Sole, R.; Onida, G., Ab initio calculation of excitonic effects in the optical spectra of semiconductors. *Phys. Rev. Lett.* **1998,** *80* (20), 4510.

44. Wei, W.; Jacob, T., Strong excitonic effects in the optical properties of graphitic carbon nitrideg-C_3N_4 from first principles. *Phys. Rev. B* **2013,** *87* (8), 085202.

45. Ramasubramaniam, A., Large excitonic effects in monolayers of molybdenum and tungsten dichalcogenides. *Phys. Rev. B* **2012,** *86* (11), 115409.

46. Ferreira, F.; Ribeiro, R. M., Improvements in the GW and Bethe-Salpeter-equation calculations on phosphorene. *Phys. Rev. B* **2017,** *96* (11), 115431.

47. Xia, C.; Xiong, W.; Du, J.; Wang, T.; Peng, Y.; Li, J., Universality of electronic characteristics and photocatalyst applications in the two-dimensional Janus transition metal dichalcogenides. *Phys. Rev. B* **2018,** *98* (16), 165424.

48. Lin, C.; Feng, X.; Legut, D.; Liu, X.; Seh, Z. W.; Zhang, R.; Zhang, Q., Discovery of Efficient Visible-light Driven Oxygen Evolution Photocatalysts: Automated High-Throughput Computational Screening of MA_2Z_4. *Adv. Funct. Mater.* **2022,** *32* (45), 2207415.

TOC Graphic